Research paper

Chondroitin sulphate and α-tocopheryl succinate tethered multiwalled carbon nanotubes for dual-action therapy of triple-negative breast cancer

Nidhi Jain Singhai [a,*], Rahul Maheshwari [b], Narendra K. Jain [a], Suman Ramteke [a]

[a] School of Pharmaceutical Sciences, Rajiv Gandhi Proudyogiki Vishwavidyalaya, Bhopal, 462 033, India
[b] School of Pharmacy and Technology Management, SVKM'S NMIMS, Green Industrial Park, TSIIC, Jadcherla, Hyderabad, 509 301, India

ARTICLE INFO

ABSTRACT

In the present investigation, novel multiwalled carbon-nanotubes (MWCNTs) tethered using alpha-tocopheryl succinate (α-TOS) and chondroitin sulphate A (CSH) (α-TOS–CSH–MWCNTs) is demonstrated. Doxorubicin (Dx) was further loaded to enhance anticancer therapeutic potential. The developed system allows to precisely targeting overexpressed CD44 receptors on triple-negative breast cancer (TNBC) specific cells. Interestingly, α-TOS- CSH-MWCNTs/Dx was found to exhibit greater cellular localization compared to non-CSH bearing formulations, revealing greater specificity. Kiton Red 620 assay revealed a significant ($p < 0.001$) decrease in MDA-MB-231 cell proliferation with GI_{50} value 0.791 ± 0.015. The apoptotic study using Annexin V/PI assay showed prominent MDA-MB-231 cell apoptosis ($53.40 \pm 3.32\%$; $p < 0.005$) when treated with α-TOS- CSH-MWCNTs/Dx in contrast to other formulations. The outcomes revealed that the combination of CSH, α-TOS and Dx could be effectively and safely used to treat TNBC.

1. Introduction

The success of cancer chemotherapy depends on selectivity, safety, and effectiveness of the treatment strategy. The situation becomes more challenging to treat triple-negative breast cancer due to difficulty in early diagnosis and aggressive nature [1,2]. Currently available treatments are limited and include chemotherapy, surgery, and radiation therapy, which may impose undesired effects [3,4]. It is challenging to deliver the anticancer molecules specifically to target cells or cancerous cells only, which cause harm to normal cells as well [5]. Selective tumor accumulation is required to enhance the therapeutic effects and to limit the side effects demands a suitable drug delivery system.

Recently, multi-walled carbon nanotubes (MWCNTs) explored widely, as they offer better drug loading, opportunities for surface functionalization, and relatively higher surface area. MWCNTs are reported as a suitable delivery platform to anticancer drugs, as most of them are hydrophobic in nature and could efficiently be loaded inside the walls of MWCNTs. Besides, MWCNTs are reported to possess strong adsorptive effects for chemotherapeutic agents, which means the effective delivery of these molecules to the effect-relevant sites. This feature makes MWCNTs a unique delivery option to load, carry, and deliver anticancer drugs with utmost efficacy. However, non-selective delivery of MWCNTs in the case of cancer may impose severe cytotoxicity to normal cells. Therefore to achieve selective delivery, precise placement and intracellular accumulation of payload is a prerequisite in the treatment of cancer cells, which demands suitable targeting ligand. Recently, Dong et al. (2017), integrated chemotherapy and photothermal therapy by delivering Doxorubicin (Dx) via CNTs, which were able to convert near-infrared radiation into heat [6]. In another investigation, Badea et al. proposed a technique to employ MWCNTs as promising tool for a drug based on platinum (cisplatin) in TNBC. The researchers revealed that cisplatin loaded MWCNTs were capable to triggers different pathways in TNBC cells which eventually enhance the understanding of TNBC cells resistance [7]. In a different study, Graham et al. reported the correlation between cells and their microenvironment using MWCNTs. They found that MWCNTs were able to stimulate the natural extracellular material to increase the cell adhesion and regulation of gene expression [8].

In the last few years, chondroitin sulphate A (CSH) has been widely explored to specifically target the CD44-receptor overexpressed cancerous cells and is well-established as effective targeting ligand [9]. Not limited to targeting, CSH has also been reported to add on anticancer effects while delivered along with anticancer agents, makes it dual role material for cancer treatment [10]. Besides, being the primary

components of extracellular matrix as well as part of many biological tissues such as bone, cartilage, skin, and blood vessels, biocompatibility is not an issue. Interestingly, CSH was reported with a remarkable role in the treatment of TNBC and therefore could be used rationally. CSH was reported to be used as a reducing and stabilizing agent for the synthesis of gold nanoparticles as well [11]. It could also be used to stabilize the MWCNTs apart from its use in active cancer-targeting [12].

It is challenging to treat TNBC using a single chemotherapeutic agent and therefore the addition of molecules, which provide the combined anticancer effect. In relation, α-Tocopheryl succinate (α-TOS) with unique anticancer properties mediated via inducing differentiation, inhibition of proliferation, and apoptosis in cancer cells appears to be a good option for adjuvant cancer treatment [13]. As reported, α-TOS does not affect the healthy cell metabolism and therefore non-toxic to normal cells which is added advantage [14].

The current investigation emphasizes on the design of the novel synergistic and targeted therapy to treat TNBC making use of Doxorubicin (Dx) as an anticancer agent, α-TOS as an anticancer adjuvant, and CHS as CD44 receptor targeting ligand delivered using MWCNTs as a drug delivery platform (Fig. 1).

The hypothesis is based on the development of selective and synergistic MWCNTs based nano-platform to attain high therapeutic efficacy in MDA-MB-231 cells whereas minimizing the untoward effects or minimum effect on normal cells. Firstly, from pristine MWCNTs differently functionalized MWCNTs such as carboxylated, acylated and aminated MWCNTs (NH$_2$-MWCNTs) were obtained in different stages. Then, in separate reactions, NH$_2$ MWCNTs were reacted with α-TOS and CSH derivative of carboxylated polyethylene glycol (PEG-COOH) to obtained α-TOS- CSH -MWCNTs. Dx was then loaded to finally obtained α-TOS- CSH -MWCNTs/Dx. Differently functionalized MWCNTs were then analyzed via conventional and state-of-the-art analytical techniques to define their size, polydispersity index (PDI), zeta potential, and surface characteristics, Dx loading and Dx release. To check the targeting efficiency of CSH, cellular internalization in MDA-MB-231 cells was observed via confocal electron microscopy. Synergistic *in vitro* anticancer effects were determined using Kiton Red 620 assay and apoptotic assay. Additionally, biocompatibility and safety of different nanoformulations were investigated via *in vitro* hemolytic assay. Stability analysis was carried out to determine the effective temperature for

prolonged storage of α-TOS- CSH -MWCNTs/Dx. The present investigation is expected to serve and assist in future experiments against other types of cancer, e.g. prostate cancer, skin cancer, lung cancer.

2. Experimental

2.1. General materials

MWCNTs (Grade: extra pure (>98%) with length 2–9 μm and radius 11–21 nm), α-TOS, Bi-arm-PEG (COOH-PEG-NH$_2$) (MW 2.1 KDa), Chondroitin sulphate A (CSH) and *N*-hydroxysuccinimide (NHS) were procured from Qualigence, Ahmedabad, India. Ethylenediamine carbodiimide hydrochloride (EDC), Sodium hydroxide (NaOH), Thionyl chloride (SOCl$_2$) were purchased from Research lab chemicals, Bangalore, India. Doxorubicin (Dx) was received as a free sample from Cadila Pharmaceuticals, Ahmedabad, India. Dimethylformamide (DMF), Ethylene Diamine (EDA), Dimethyl Sulfoxide (DMSO), and Dialysis membranes with molecular cut off 12,000–14000 kD and 1000–2000 kD were purchased from Qualigence, Hyderabad, India. The rest of the materials like ethanol, acetic acid, MilliQ water, and hydrochloric acid, were procured from certified vendors and were of analytical rank.

2.2. Cell line and cell culture experiment materials

MDA-MB-231 cells (American Type Culture Collection; ATCC) were procured from National center for cell science (NCCS), Pune, India. Trypsin-ethylene diamine tetra-acetic acid, Dulbecco's modified Eagle medium (DMEM), antibiotic antimycotic 100X solution (penicillin, streptomycin amphotericin B combination), heat-inactivated fetal bovine serum, Kiton Red 620 dye, and Alexa Fluor 488 kit were procured from Gibco, Thermo fisher scientific, Bangalore, India.

2.3. Carboxylation, acylation and subsequent amination of MWCNTs

Firstly, pristine MWCNTs were oxidized following earlier reported protocols. Briefly, 200 mg MWCNTs were dispersed in a beaker containing a mixture of H$_2$SO$_4$ and HNO$_3$ (3:1 v/v) using ultrasonicator (PCI Instruments, Bhopal, India) for 10 min following refluxing at 85 °C using temperature sensor enabled magnetic stirrer (Remi 1MLH, Mumbai,
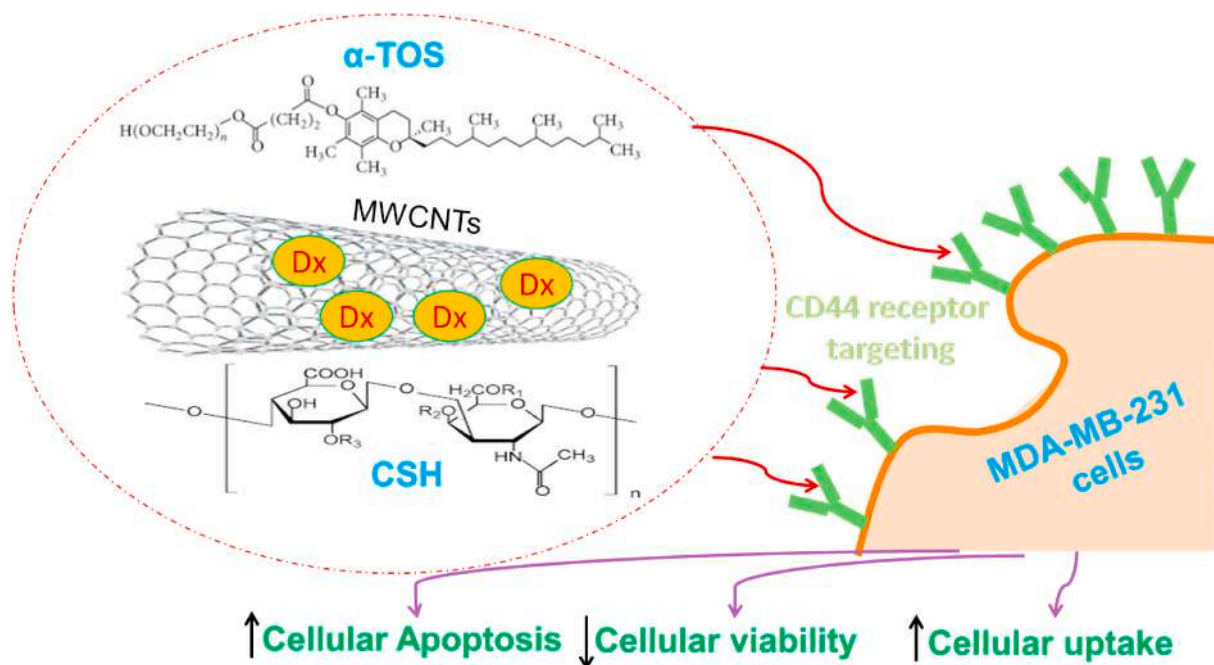

Fig. 1. Anti-TNBC effect mediated by CSH, and α-TOS attached and Dx loaded MWCNTs.

India) at 850 rpm for 180 min [15]. Then, resulting dispersion was washed 5–6 times via repetitive centrifugation (10 min cycle with 5 min off time; 12,000 rpm; Remi Labs, Hyderabad, India) using millipore water. The process continued until the pH reached between 5.2 and 6.2 ranges. The obtained dispersion was further centrifuged at 11,000 rpm (15 min) to remove all the traces of acidic materials, the supernatant was discarded and the final product was collected as carboxylated MWCNTs (COOH-MWCNTs) which was further utilized to get acylated MWCNTs. Briefly, 140 mg of air-dried COOH-MWCNTs was dissolved in $SOCl_2$: DMF (20:1 v/v) at 75 °C for 24 h using magnetic stirrer operated at 350 rpm [16]. To remove the traces of $SOCl_2$, the as-obtained MWCNTs were subjected to centrifugation at 12,000 rpm for 10 min (6X) using THF. The finally collected dark black residues of acylated MWCNTs was dried under an oven (Vacuum oven; JS Instruments, Indore, India) at 30 °C and further used to obtain NH_2-MWCNTs. For amination, the as dried acylated MWCNTs (100 mg) were reacted with excess EDA at 110 °C for 72 h continued until hydrogen chloride gas was evolved [17]. At the point, hydrogen chloride gas formation stopped, MWCNTs dispersion was collected and subjected to washing (using ethyl alcohol) via centrifugation at 12,000 rpm for 10 min (several cycles until the excess of EDA was eliminated. Finally obtained aminated MWCNs, were dried for 24 h in a vacuum oven to get free-flowing residue for further use.

2.4. Attachment of α-TOS and CSH to NH_2-PEG-COOH CSH

To activate –COOH group of α-TOS, 24.2 mg; 0.000235 mol of α-TOS was reacted (under magnetic stirrer at 400 rpm; 3 h) with pre-dissolved EDC (8.68 mg, 0.0000235 mol) and NHS (9.16 mg, 0.0000235 mol) in 4 mL DMSO in a round bottom flask [18]. Then, the activated α-TOS (1.5 molar equivalents) progressively incorporated (under stirring at 700 rpm) to 58 mg (0.000025 mol) NH_2-PEG-COOH pre-dissolved in 10 mL of DMSO and kept aside for 24 h. Then, it was collected and dialyzed (MWCO 1-2 KDa) against phosphate buffer (pH 7.4) and water sequentially for three days each to wash off the excess reactants followed by lyophilization (Pre-treated with cryoprotectant; FD508; IIShinBio-Base; South Korea) to produce fine powder of α-TOS-PEG. A similar reaction was carried out to conjugate CSH to NH_2-PEG-COOH. In brief, –COOH group of CSH, 22.5 mg; 0.0000235 mol of CSH was reacted (under magnetic stirrer at 400 rpm; 3 h) with pre-dissolved EDC (8.68 mg, 0.0000235 mol) and NHS (9.16 mg, 0.0000235 mol) in 4 mL DMSO in a round bottom flask. Then, the activated CHS (1.5 molar equivalents) was gradually incorporated (under stirring at 700 rpm) to 58 mg (0.000025 mol) NH_2-PEG-COOH pre-dissolved in 10 mL of DMSO and kept aside for 24 h. Then, it was collected and dialyzed (MWCO 1-2 KDa) against phosphate buffer saline (PBS) and water sequentially for 3–4 days each to wash off the excess reactants followed by lyophilization (Pre-treated with cryoprotectant) to produce fine powder of CSH-PEG.

2.5. Preparation of α-TOS–CSH–MWCNTs

To synthesize α-TOS- CSH-MWCNTs, first –COOH ends of α-TOS-PEG (18.6 mg) were stirred (for activation) with 2.5 M equals of EDC (30.2 mg, 0.0001865 mol) and NHS (32.4 mg, 0.0001872 mol) as crosslinker (in 6 mL water) for 2–3 h at 400 rpm. In the same way,-COOH group of CSH-PEG (14.6 mg) were stirred (for activation) with 2.5 molar equivalents of EDC (34.4.2 mg, 0.0001879 mol) and NHS (39.2 mg, 0.0001879 mol) as coupler (in 6 mL water) for 2–3 h at 400 rpm. Afterward, the –COOH activated α-TOS-PEG and CSH-PEG was added slowly to NH_2/MWCNTs (60.2 mg in 10 mL water) with continuous stirring (24 h). Finally, the dispersion (MWCO 12–14 kDa) was dialyzed against PBS for 2 days and with water for a day for purification followed by lyophilization to get powdered α-TOS–CSH–MWCNTs.

2.6. Characterization of different MWCNTs conjugates

2.6.1. UV spectroscopy and FTIR spectroscopy

Carboxylated/acylated MWCNTs, NH_2/MWCNTs, α-TOS, CSH, Dx, α-TOS-MWCNTs, CSH-MWCNTs and α-TOS- CSH-MWCNTs were analyzed via UV vis spectroscopy (1700, Shimadzu, Tokyo, Japan). Prior to analysis, samples were appropriately diluted with purified water, and the experiment was performed in triplicate. A similar set of formulations were analyzed using FTIR spectroscopy (Shimadzu, Japan) too. For the experiments using FTIR, the scanning range selected was 3900–600 cm^{-1}.

2.7. 2^1H nuclear magnetic resonance (^1H NMR) spectroscopy

Carboxylated/acylated MWCNTs, NH2/MWCNTs, α-TOS, CSH, Dx, α-TOS-MWCNTs, CSH-MWCNTs and α-TOS- CSH-MWCNTs were analyzed via NMR spectroscopy (Bruker India, Hyderabad, India). D_6-DMSO was used as an experiment solvent.

2.8. Dx loading

Dx was loaded using the equilibrium dialysis technique as previously reported [19]. Dx (2 mg/mL) pre-dissolved in the solvent mixture (acetone + TEA) and then kept under magnetic stirring (45 min). Dx (1 mg/mL) loading was then carried out in PBS (pH adjusted to 7.4) under continuous stirring for 45 h under dark (no light). The final product was purified and excess Dx was removed using repetitive centrifugation (10 min cycle; 5500 rpm). The absorbance was measured at 476 nm using UV vis spectrophotometer (UV detector, 1700, Shimadzu, Tokyo, Japan). Similarly, NH_2/MWCNTs, α-TOS-MWCNTs and CSH-MWCNTs were loaded with Dx. Dx loading was estimated via the following equation.

$$\% \text{ Loading efficiency} = \frac{LD - FD}{LD} \times 100 \qquad (1)$$

LD and FD stands for loaded and free Dx, respectively.

2.9. Surface characterization

2.9.1. Dynamic light scattering measurement

Size, polydispersity index (PDI), and surface charge of different MWCNTs formulations were analyzed in using zetasizer (Malvern, UK). Appropriate dilutions of the samples were made, prior to measurement.

2.9.2. Transmission electron microscopy (TEM)

The surface topography of the modified MWCNTs was characterized using TEM (Oregon, USA) at an accelerated voltage of 20 kV at a magnification of 4000. Prior to measurement, formulations were negatively stained with a 1% w/v aqueous solution of phosphotungustic acid.

2.10. In vitro drug release studies

Dx release was measured at pH 7.4 (PBS) and pH 5.0 (acetate buffer) to simulate the normal physiological conditions and acidic tumorous conditions. Dx-loaded MWCNTs were separately filled in a hermetically sealed dialysis bag (12-14 KDa) attached with the receiver compartment. The temperature was set to 37±[fx]0.5 °C. At the pre-designated time, (1, 4, 8, 12, 24, 48, 72, 96 and 120 h) aliquots (0.5 mL) were withdrawn from the receiver compartment and the same amount of media was transferred back. UV–Vis spectroscopy was used to determine the released Dx at 476 nm [20].

2.11. Cytotoxicity assay using SRB dye

Kiton Red 620 assay was employed to determine the anti-cancer potential of different MWCNTs using MDA-MB-231 cells. Briefly, cells

were cultured in 96-well plates (5×10^3 cells/well) for 24 h following incubation for 48 h. Then, cells were added with 0.01–100 μg/mL of different MWCNTs formulations and then fixed using 50 μL of cold 55% w/v TCA followed by incubation for 1 h at 4 °C. Kiton Red 620 (50 μL) at 0.05% (w/v) in diluted acetic acid was then added to each well followed by incubation for 1 h. The residual dye was removed by 2 or 3 washing with diluted acetic acid, and then the plates were dried. Meanwhile, the bound dye washed off using 10 mM Tris buffer pH adjusted to 10.5. The values of GI_{50} were calculated via a non-linear regression method using GraphPad Prism version 6.01™software and the absorbance values were set at 490 nm.

2.12. Cellular uptake analysis

To determine cellular internalization, seeded (2.5×10^5 cells per 12-well plate) and 24 h incubated MDA-MB-231 cells were treated with GI_{50} concentration of control, Dx, and Dx loaded aminated, α-TOS-MWCNTs, CSH -MWCNTs, and α-TOS- CSH -MWCNTs for 24 h. Then, the media was aspirated out and washed using PBS for 2–3 times. After that, cells were stained with DAPI (5 μg/mL for 30 min). The alteration in the nucleus was seen using a confocal laser scanning microscope (CLSM: Leica TCS SP5 AOBS, Leica, Germany) at an excitation and emission wavelength of 365 nm and 460 nm, respectively.

2.13. Apoptotic assay using Alexa Fluor® 488 kit

For the apoptotic assay, MDA-MB-231 cells were harvested and each well-equipped with a population of 2.5×10^5 cells (pre-treated with their respective GI_{50} concentration for 24 h) treated using Alexa Fluor® 488 kit. Afterward, binding buffer (100 μL) was added to the individual well. Then, samples were incubated under dark conditions for few mins. Then, 300 μL 1X binding buffer was incorporated into each well and analyzed via flow cytometry (Bio Rad System, USA). 10,000 cells in the gated region were measured as the minimum number of cells.

2.14. Blood compatibility assay

To access the blood compatibility, control, Dx, and modified MWCNTs formulations were added (at their GI_{50} concentration) to the collected and heparinized mouse blood into storage vials [21]. Different vials were then subjected to shaking followed by centrifugation at 2200 rpm for 12 min to get the supernatant, which was further measured using UV spectroscopy at 540 nm % hemolysis for each samples were calculated using equation (2).

$$\% \ Haemolysis = \frac{Absorbance \ of \ sample - Absorbance \ of \ blank}{Absorbance \ of \ positive \ control - Absorbance \ of \ blank}$$
$$\times 100 \qquad (2)$$

Collected RBCs were treated with Triton X 100 and normal saline separately to serve as positive control to be used in the calculation.

2.15. Stability study

The stability of NH_2-MWCNTs/Dx and α-TOS–CSH–MWCNTs/Dx were analyzed after dispersing (0.1 g/mL) MWCNTs and Dx equivalent to ~15 mM (kept in amber color vials) at two different temperatures viz $5 \pm 1/30 \pm 2$ °C for 120 days. At time points Day 1, 30, 60, 90, and 120 samples were collected and measured for possible changes in average size, PDI, surface charge, and % Dx retention.

2.16. Statistical analysis

One-way analysis of variance (ANOVA) with a Tukey–Kramer multiple comparison Post-test and two-way ANOVA with Bonferroni post-test was used for different experiments. GraphPad Prism was used for

data analysis. The values $p < 0.01$ and $p < 0.001$ were considered as significant/highly significant as that considered as non-significant ($p > 0.05$).

3. Results and discussion

TNBC is an aggressive cancer type that tests negative for progesterone receptors, estrogen receptors, and excess HER2 protein [22]. TNBC is more aggressive and tends to be of a higher grade than other types of breast cancers [23]. There are few targeted medicines for the treatment of TNBC and is typically treated with a combination of surgery, radiation therapy, and chemotherapy [24]. Hence, targeted, efficient and safe therapy for treating TNBC is of utmost importance and also for the treatment of TNBC current focus areas are for the development of the majority of nanomedicines [7,8]. In the last few years, for the delivery of small therapeutic molecules, MWCNTs among the carbon-based materials have been explored largely due to their magnificent properties including mechanical strength and high drug loading [25]. MWCNTs are allotropes of carbon that are hollow and cylindrical with high aspect ratio i.e. length to diameter ratio. They are made up of multiple rolled layers of concentric graphene nanotubes inside the other nanotubes. The use of MWCNTs is extensively reported in nanotechnology for the theragnostic applications i.e. for the diagnostic test that identifies the diseases or abnormal conditions in the patient and targeted drug therapy to treat the condition [26]. Natural high hydrophobicity of carbon nanotubes (CNTs) is the main reason for restriction behind their use, which may result in accumulation leading to the production of toxicity [27]. MWCNTs due to their inorganic residues, diameter, shape, and size are known to produce severe pulmonary toxicity [28]. Particularly, in cancer, tall MWCNTs may diminish them to accumulate at the desired site of action i.e. cancer cells. Due to less utilization, it may result in accumulation leading to toxicity production. To reduce the toxicity of MWCNTs surface functionalization may be used in terms of amination, carboxylation, and acylation. Surface modification results in the accessibility of phenolic, carboxylic and lactone groups on the sidewall surface of MWCNTs due to which the suspendability or solubility in the aqueous medium increases significantly [29].

3.1. Surface modification of MWCNTs

As can be seen in Fig. 2, reaction begins from pristine MWCNTs and upon reacting with acids (mixture of H_2SO_4 and HNO_3) oxidation of MWCNTs takes place and converted to COOH-MWCNTs. Upon reacting with $SOCl_2$ (acylating agent) in DMF, COOH-MWCNTs MWCNTs were converted to acylated MWCNTs, which upon reacting with EDA (for the attachment of amine groups) are finally converted into NH_2-MWCNTs. Simultaneously, COOH-PEG-NH_2 was reacted with EDC and NHS (as coupling reagents) separately with α-TOS and CSH to obtained α-TOS-PEG-COOH and CSH-PEG-COOH, respectively. In a final reaction, α-TOS-PEG-COOH and CSH-PEG-COOH were reacted again with NH_2-MWCNTs in DMSO in the presence of EDC and NHS to obtain α-TOS-CSH-MWCNTs. The reason for adding CSH along with α-TOS was to enable the MWCNTs to specifically internalize into CD44 receptors overexpressed cancerous cells to achieve efficient targeting.

3.2. UV vis spectroscopic analysis

Due to the presence of free Π electrons, pristine MWCNTs displayed absorbance in the UV–Vis range and as can be seen in Fig. 3A, a characteristic peak at 224 nm was observed. Conversion of pristine MWCNTs to COOH-MWCNTs confirmed as two main absorption peaks of oxidation were observed. Peak at ~259 nm corresponding to the prominent π-plasmon absorption peak resulted from the total excitation of the π-electrons upon carboxylation. Also, a non-resonant flattened curve observed as a second feature due to contributions from both MWCNTs and other materials. Similarly, the characteristic peak for acylation and
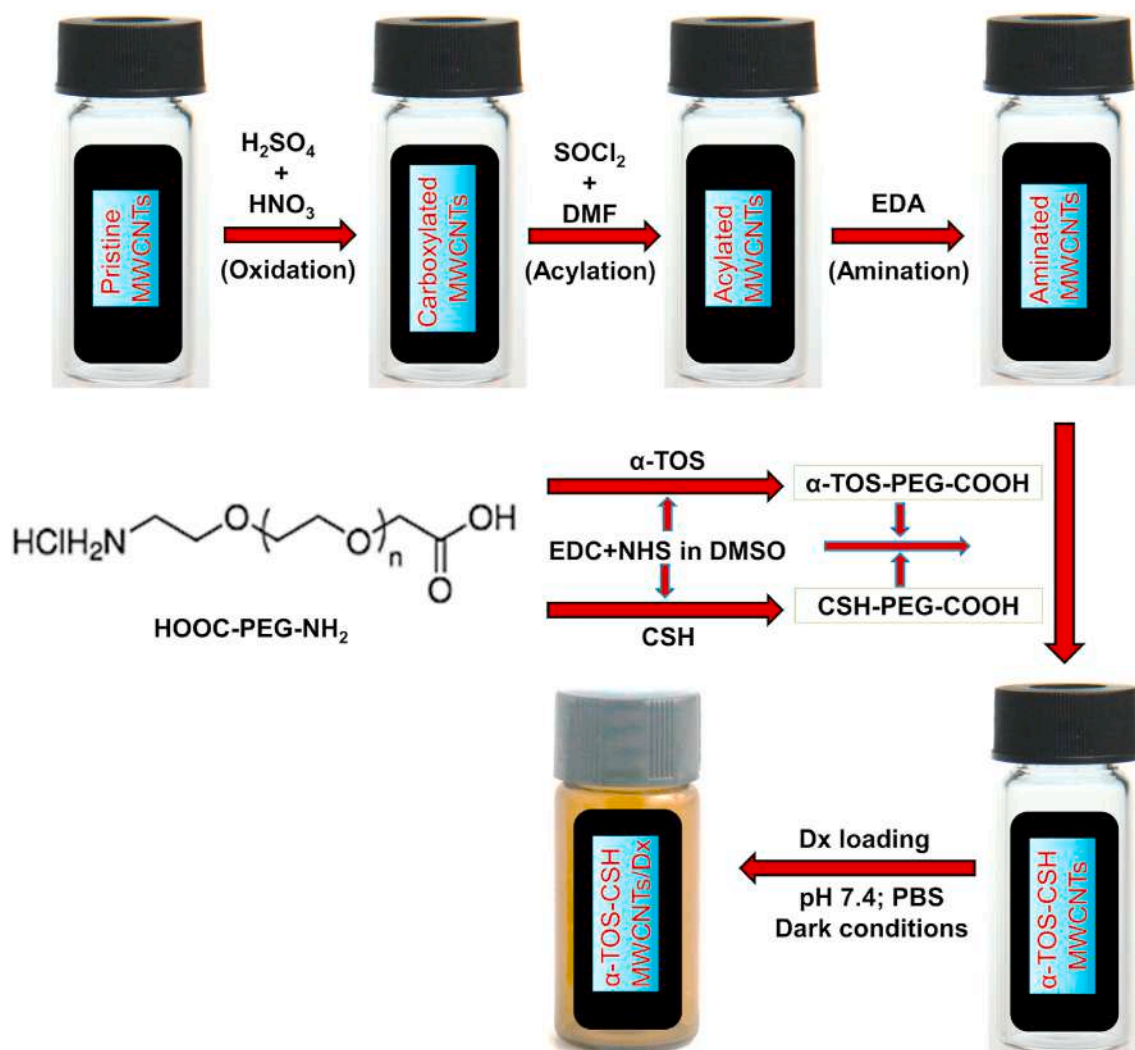
Fig. 2. Subsequent synthetic reactions leading to the formulation of α-TOS- CSH-MWCNTs/Dx. *Next, α-TOS-PEG-COOH and CSH-PEG-COOH (produced in separate reactions) were reacted with NH2-MWCNTs to form α-TOS-CSH-MWCNTs. Finally, the Dx was loaded to get α-TOS-CSH-MWCNTs/Dx.*

subsequent amination was observed at ∼231 nm and ∼281 nm, respectively. In particular, chloride substitution in carbonyl group, carrying a lone pair of electron brings π-π* transition, in case of acylated MWCNTs. Because of the inductive effect which tightens lone pair electrons resulted into the shifting of the peak at shorter wavelength. Our findings are in good correlation with the previously reported literature [19,30]. Further, characteristic peaks at 285 nm and 440 nm were observed for α-TOS and CSH, respectively. Further, peaks at 335 nm and 450 nm authenticate the attachment of α-TOS and CSH to MWCNTs. The characteristic peak of Dx at 510 nm disappears with α-TOS–CSH–MWCNTs/Dx confirmed successful loading of Dx into nanotube architect.

3.3. FTIR analysis

FTIR was used as another tool to identify structural changes in different modified MWCNTs based on functional group peak alterations. As can be seen in Fig. 3B, alteration of pristine MWCNTs to COOH-MWCNTs confirmed via peak at 3459 cm^{-1} and 1702, respectively for the O–H/C$=$O bending. Similarly, peaks at 2912 cm^{-1} and 777 cm^{-1}respectively for C–H stretching and C–Cl stretching verified the acylation and formation of acylated MWCNTs. Further, the formation of NH$_2$-MWCNTs from acylated MWCNTs was identified by verifying the readings obtained at 3410 cm^{-1} and 1322 cm$^{-1,}$ respectively for N–H

and C–H stretching. Besides, amide bond formation was identified by noticing C$=$O stretching at 1661 cm^{-1}. In a simultaneous reaction to obtain α-TOS-PEG, bis-arm PEG with –COOH and –NH$_2$ groups on each side was reacted with α-TOS along with EDC and NHS and creation of α-TOS-PEG was verified at 3450 cm^{-1}, 1771 cm^{-1}, and 1633 cm^{-1} peaks, analogous to N–H/C$=$O stretching of acidic groups. Along the side, in a similar type of reaction to confirm the formation of CSH-PEG peaks were observed at 3331/1738/1668 cm^{-1} and could be denoted as N–H/C$=$O stretching of acid/C$=$O stretching of amide. Next, NH$_2$-MWCNTs were conjugated with α-TOS-PEG and CSH-PEG using two different reaction vessels and the formation of α-TOS- CSH-MWCNTs was verified by observing the peaks at 3450/3290/1141/1077 cm^{-1}, corresponding to N–H/C–O stretching of ether. Moreover, the loading of Dx into α-TOS- CSH-MWCNTs was confirmed as peaks appeared at 1641 cm^1 and disappeared at 1591 cm^{-1} and 1621 cm^{-1} (N–H), which existed in plain Dx FTIR.

3.4. ^1H NMR analysis

Being the state of the art technique for structure elucidation and analysis NMR was used to fetch modification to MWCNTs at different levels (Fig. 3C). Alteration of pristine MWCNTs to COOH-MWCNTs didn't generate any comparative proton signal, as already reported in the earlier research [30]. The formation of NH$_2$-MWCNTs was confirmed
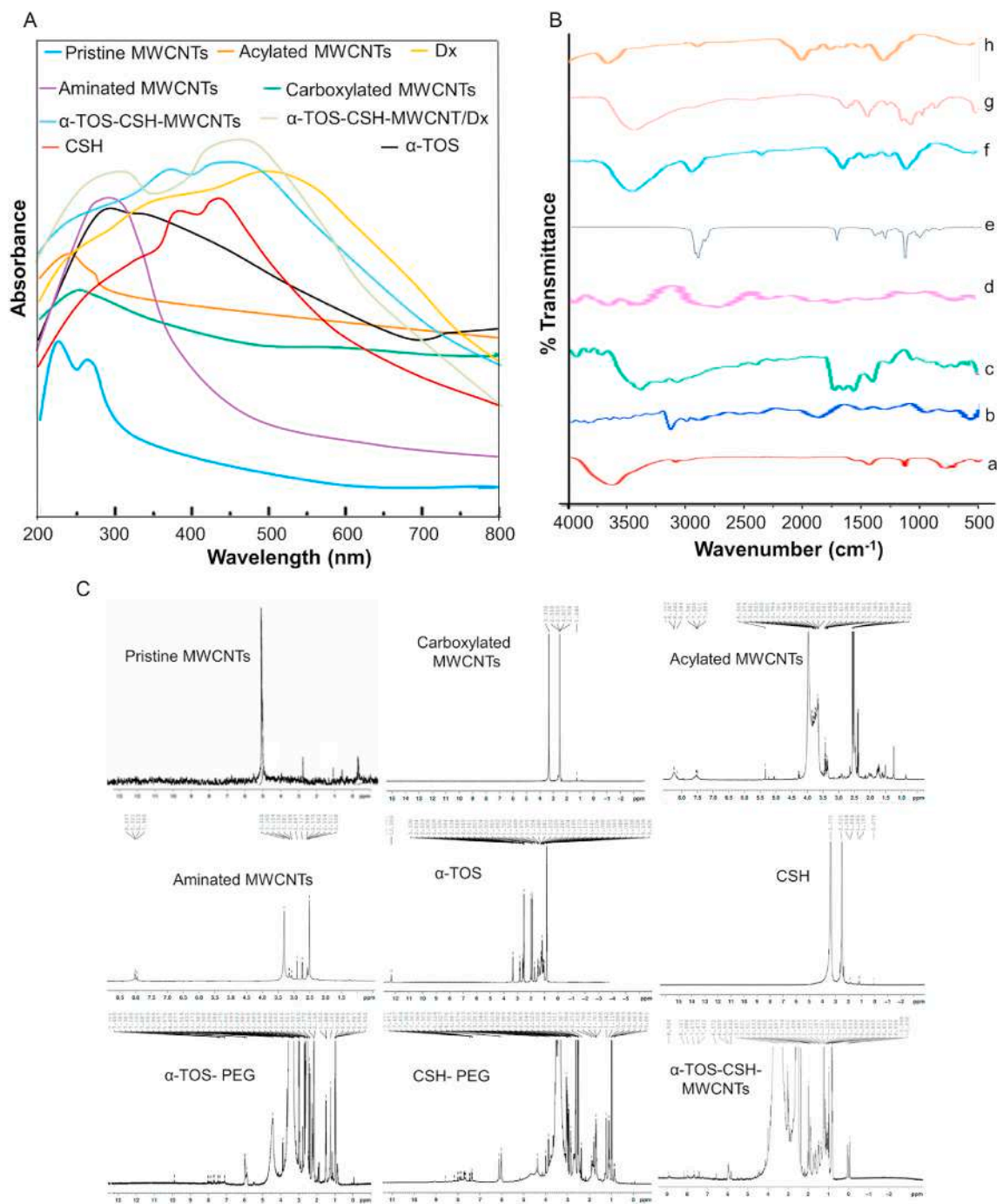
Fig. 3. (A) UV spectroscopic analysis of different formulations to characterize them on the basis of absorption pattern (B) FTIR analysis of a. COOH-MWCNTs, b. acylated MWCNTs, c. NH2-MWCNTs, d. CSH, e. α-TOS, f. α-TOS- CSH-MWCNTs, g. Dx h. α-TOS- CSH-MWCNTs/Dx. FTIR served as a reliable technique for verifying the attachment to MWCNTs at different levels (C) 1H NMR analysis. NMR was used for authentication of MWCNTs modification at different levels. *Results are represented as Mean ± SD (n = 3).*

via CH$_2$- proton signals observed around 1–3 ppm stand for amine conjugation. Conjugation of α-TOS with bis-arm PEG was verified by obtaining proton peaks at 0.820–2.212/2.654–2.765 ppm respectively for 2 protons of methylene on the B position of benzene. Similarly, CSH peaks recorded at 1.7–2.3 ppm and 4.31–5.28 ppm relate, respectively to acetamido/methylene groups of CSH. Sequentially the attachment of bis-arm PEG with α-TOS and CSH in two different reactions was confirmed via noticing the characteristic proton peaks between 7.0–7.4 ppm. Finally, α-TOS-PEG and CSH-PEG was attached to NH$_2$-MWCNTs and the development of α-TOS- CSH-MWCNTs verified after getting proton peaks related to α-TOS and CSH whereas shift around 3.0 ppm

reflect that the aromatic 1° amine is present.

3.5. Surface parameter analysis

3.5.1. Size, PDI and surface electric charge measurement

Being the important properties in determining the efficacy and safety of the MWCNTs, size, and surface charge were determined. As can be seen in Fig. 4A–E, a gradual increase in size was observed with each step of synthesis with newer products. Lowest size observed with COOH-MWCNTs (105.1 ± 1.62 nm) and highest with α-TOS–CSH–MWCNTs/Dx (132.1 ± 1.13 nm) with a total increment of about 25.68 ± 1.47% in
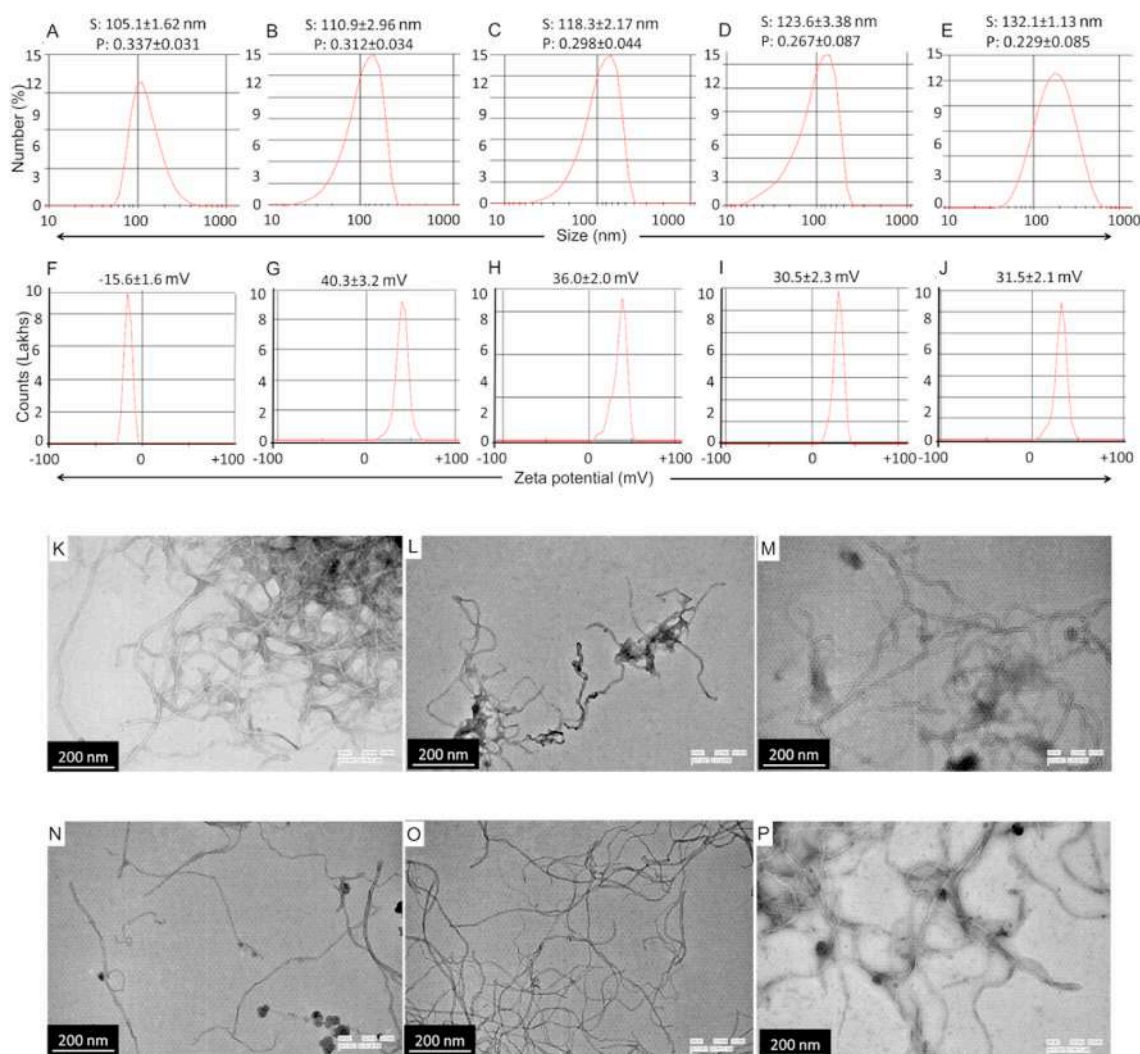
Fig. 4. Size (S) and PDI (P) determination of (A) COOH-MWCNTs (B) NH$_2$-MWCNTs/Dx(C) α-TOS-MWCNTs/Dx (D) CSH-MWCNTs/Dx (E) α-TOS- CSH-MWCNTs/ Dx. Surface charge of (F) COOH-MWCNTs (G) NH$_2$-MWCNTs/Dx (H) α-TOS-MWCNTs/Dx (I) CSH-MWCNTs/Dx (J) α-TOS–CSH–MWCNTs/Dx. and TEM photomicrograph of (K) pristine MWCNTs (L) COOH-MWCNTs (M) NH$_2$-MWCNTs/Dx (N) α-TOS-MWCNTs/Dx (O) CSH-MWCNTs/Dx (P) α-TOS–CSH–MWCNTs/Dx. *Scale bar for Fig. 4 (K)–(P) is 200 nm. Results are represented as Mean ± SD (n = 3).*

the subsequent steps of synthesis and conjugation via forming differently modified MWCNTs. A gradual increase in size from NH$_2$-MWCNTs/Dx, α-TOS-MWCNTs/Dx, and CSH-MWCNTs/Dx could be attributed to sequential transfer of amino group, α-TOS, and CSH ligand, respectively. Another reason could be the Dx loading which may increase the size of MWCNTs formulations. All the MWCNTs formulations were found homogeneous with PDI values ranging from 0.337 ± 0.031 to 0.229 ± 0.085 from COOH-MWCNTs to α-TOS–CSH–MWCNTs/Dx. (Fig. 4A–E). Improvement in PDI with sequential synthesis steps explaining the role of ligand attachment in gaining homogeneity. Furthermore, significant shifts from −15.6 ± 1.6 mV to +40.3 ± 3.2, in zeta potential value from COOH-MWCNTs to aminated-MWCNTs ascribed the conjugation of a highly positive amine group on the surface of the nanotubes, which ultimately increased the surface charge (Fig. 4F–G). Afterward attachment of α-TOS and CSH to NH$_2$-MWCNTs slightly alter the charge towards the downside, which may be due to the nature of individual ligands (Fig. 4H–I). Finally, α-TOS–CSH–MWCNTs/ Dx revealed a zeta potential of 31.5 ± 2.1, which is significantly (*p < 0.001*) different from COOH-MWCNTs (Fig. 4J).

3.5.2. Analysis of surface topography

Surface topography was determined using TEM to analyze the

changes upon formation of different MWCNTs in subsequent synthesis pathways as described in Fig. 4. As can be seen in Figure 4L surface of MWCNTs appears to shorten upon conversion to NH$_2$-MWCNTs attributing to the removal of metallic traces in subsequent steps from carboxylation to acylation and amination (Fig. 4K-L). Furthermore, surface alteration in α-TOS-MWCNTs and CSH-MWCNTs might be due to the attachment of ligands on the surface of MWCNTs, as shown in Figure M–N. Changes were also observed after the formation of α-TOS–CSH–MWCNTs and subsequent loading of Dx into it (**Figure O–P**).

3.6. Drug loading

The Dx loading capacity of NH$_2$-MWCNTs, α-TOS-MWCNTs, CSH-MWCNTs, and α-TOS–CSH–MWCNTs were measured via the equilibrium dialysis method. As compared to NH$_2$-MWCNTs (52.23 ± 2.11%), α-TOS-MWCNTs (62.32 ± 3.12%), and CSH-MWCNTs (63.65 ± 3.67%); α-TOS–CSH–MWCNTs were found to hold highest amount of Dx (74.65 ± 2.87%). Particularly, α-TOS-MWCNTs and CSH-MWCNTs were found to have almost equal capacity to load the Dx (*p > 0.05*) but greater than NH$_2$-MWCNTs (*p < 0.01*). α-TOS–CSH–MWCNTs were found to load the highest amount of Dx and superior (Fig. 5 (A); *p < 0.001*) as compared
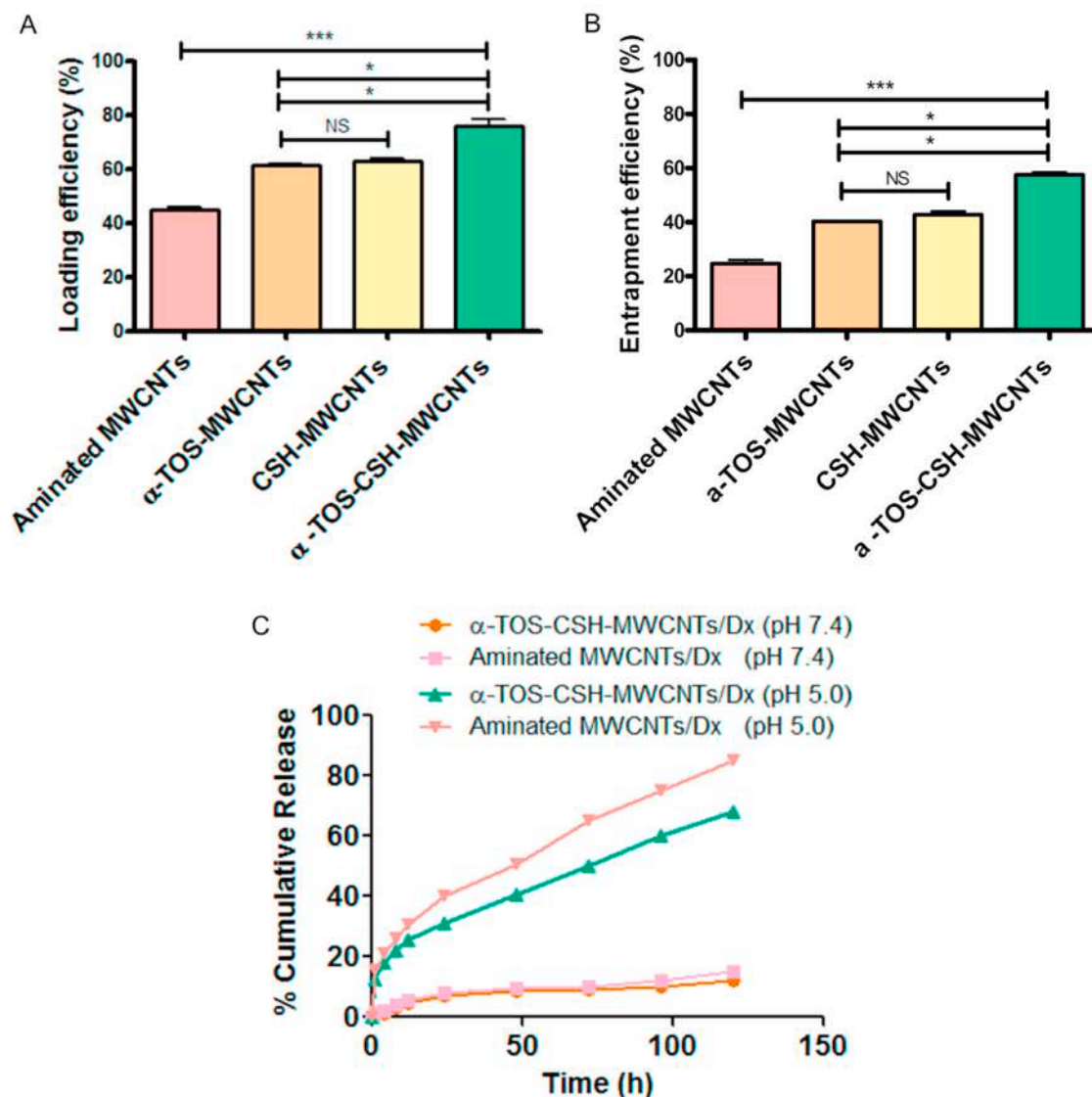
Fig. 5. (A) Loading efficiency and (B) entrapment efficiency of NH_2-MWCNTs, **α-TOS-MWCNTs, CSH-MWCNTs, and α-TOS-CSH-MWCNTs. (C) % cumulative release of Dx in 120 h from α-TOS-CSH-MWCNTs/Dx and** NH_2-**MWCNTs/Dx at** pH **7.4 and 5.0 corresponding to physiological and acidic environment.** *Results are represented as Mean* $\pm$ *SD (n = 3).*

to other MWCNTs formulations attributed to higher π-π stacking interaction, H-bonding and hydrophobic interactions owing to the ring structure of the Dx. Similarly, entrapment efficiency was also calculated as presented in Fig. 5 (B).

3.7. Drug release kinetics

The Dx release profile of α-TOS–CSH–MWCNTs/Dx was accessed at pH 7.4 (PBS) and pH 5.0 (SAB) and samples were withdrawn at different time points in 120 h study. At pH 7.4 15.67 $\pm$ 2.11% and 12.11 $\pm$ 1.34% (p < 0.05) Dx was released from NH_2-MWCNTs/Dx and α-TOS–CSH–MWCNTs/Dx, respectively. However, at acidic pH, Dx release was found provoked from α-TOS–CSH–MWCNTs/Dx and almost 74.23 $\pm$ 3.54% Dx entered into receiver media (SAB) in 120 h. The release of Dx was even faster from NH_2-MWCNTs/Dx and almost 87.76 $\pm$ 3.78% Dx was released in 120 h (Fig. 5 (C)). The rate of Dx release exhibited a non-linear arrangement being faster at the initial few hours and then follows the sustained release pattern. At both the pH environments, Dx release from NH_2-MWCNTs displayed a quicker rate of release in comparison to α-TOS–CSH–MWCNTs/Dx. Findings revealed

that Dx has a prominent release at acidic pH condition as compared to alkaline condition and therefore provides an opportunity for the better and precise therapeutic effect to treat TNBC. Literature also suggests that Dx shows pH centered solubility and protonation of its daunosamine groups at lower pH conditions could also be attributed to mimicking the release rate at pH 5.0. Besides, as a fact, π-π stacking interaction is prominent at alkaline pH conditions and becomes weaker as pH moves towards lower end (acidic pH), which prompted the dissociation of Dx from MWCNTs. This is a critical parameter as the pH of tumorous tissue is acidic. MWCNTs also served a crucial role in holding the Dx for the prolonged period being hydrophobic in nature, which also restricts Dx release from its architect. For targeted chemotherapy, pH-dependent release as shown in our case could play a major role to treat TNBC. Our findings could be correlated to those observed by Cao et al. wherein they found over 50% of Dx released at acidic pH in 70 h from hyaluronic acid decorated MWCNTs [30].

3.8. Cytotoxicity assay

Kiton Red 620 assay was employed to test the anticancer potential of

Dx, Dx loaded NH$_2$-MWCNTs, α-TOS-MWCNTs, CSH-MWCNTs and α-TOS–CSH–MWCNTs employing MDA-MB-231 cell. Kiton Red 620 assay is superior to MTT assay as it is based on the stoichiometric binding of the dye to basic amino acids under a slightly acidic environment whereas MTT assay involves the metabolic activity of the cells. Kiton Red 620 assay measures the intensity of color, which is directly proportional to the living cells in the suspension. Growth inhibition (GI$_{50}$) values of all the formulations measured (Fig. 6 (A). As can be seen in Fig. 6 (B) (data interpretation using Image J (1.46r version) software) Dx alone (GI$_{50}$; 2.786 ± 0.141) and Dx loaded NH$_2$-MWCNTs (GI$_{50}$; 1.942 ± 0.031) were found to be less effective as contrast to α-TOS-MWCNTs/Dx (GI$_{50}$; 1.341 ± 0.023; p < 0.001) and CSH-MWCNTs/Dx (GI$_{50}$; 1.221 ± 0.0387; p < 0.001). Whereas,α-TOS and CSH when clubbed together (α-TOS–CSH–MWCNTs/Dx) was found with lowest GI$_{50}$; 0.791 ± 0.013; p < 0.001 and therefore exert maximum cytotoxicity to MDA-MB-231 cells. The probable reason behind the findings may be the attachment of dual ligands to the MWCNTs that actually increases the cellular entry of the α-TOS–CSH–MWCNTs/Dx, which leads to the availability of high concentration of Dx inside the cells to intermingle with the DNA pairing and subsequent cell death. Intracellular accumulation of Dx via enhanced cellular uptake decreases the GI$_{50}$ values and thereby inhibits cell growth. Besides, the fact that surface alteration via chemical modification of MWCNTs, which ultimately leads to minimizing the aggregation/bundling cannot completely rule out and also contribute to enhanced therapeutic efficacy of synergistic treatment. Our results are in good correlation with those obtained by Yan et al., who developed and tested folic acid targeted polyethylene glycol and dendrimer modified MWCNTs [31].

3.9. Cellular internalization experiment

To access the effective ligand binding, cellular internalization of ligand (TOS and CSH) attached MWCNTs was assessed against NH$_2$-MWCNTs/Dx and Dx alone. Findings suggest that Dx alone and NH$_2$-MWCNTs were unable to reach inside the cells and found with rare and low cellular internalization, respectively. Cellular uptake enhanced with α-TOS- MWCNTs/Dx and CSH-MWCNTs/Dx as can be seen in Fig. 7. Further improvement in cellular localization was found with α-TOS–CSH–MWCNTs/Dx as compared to α-TOS- MWCNTs/Dx and CSH-MWCNTs/Dx attributed to the combined effect of α-TOS and CSH.

Findings justify lower GI value obtained with α-TOS–CSH–MWCNTs/Dx in Kiton Red 620 assay. Oommen et al. proposed multifunctional hyaluronic acid and CSH nanoparticles and explored the cellular uptake via CD44 receptor targeting leading to immunological evaluations [32].

3.10. Apoptosis analysis

To determine the % total cellular apoptotic ratio (% TCAR), MDA-MB-231 cells were treated for 24 h with different MWCNTs considering their respective GI values. As can be seen in, Fig. 8 (A-F), lower % TCAR value was observed with Dx and NH$_2$-MWCNTs/Dx17.20 ± 1.22%; p < 0.001 and 19.7 ± 2.11%; p < 0.001. In contrast to Dx and NH$_2$-MWCNTs/Dx, improved % TCAR was detected with α-TOS-MWCNTs/Dx (21.81 ± 3.13), and CSH-MWCNTs/Dx (34.62 ± 2.43). Analysis using Image J software is presented in Fig. 8 (G). Importantly, α-TOS–CSH–MWCNTs/Dx showed maximum% TCAR (50.51 ± 4.33%; p < 001) suggesting the higher nuclear fragmentation and condensation in treated MDA-MB-231 cells. This might be due to the dual ligand effect, which enables the formulation to localize inside cells and thereby Dx exerted its anticancer potential. Besides, anticancer nature of CSH and α-TOS must also be accounted for achieving synergistic effects and cannot be completely ruled out. Conclusively, α-TOS and CSH mediated delivery of Dx via MWCNTs were able to achieve higher anticancer effects in comparison to other tested formulations. Similarly, Ozgen et al., developed a glycopolymer based MWCNTs delivery system and found that total apoptotic cells were significantly higher than cells treated with free Dx, as we previously reported [33].

3.11. Determination of blood compatibility

Blood compatibility assay was used to determine the safe nature of MWCNTs based formulations. Results showed the nontoxic nature of different MWCNTs. No significant interference (low hemolytic percentage) was observed with all the tested formulations during the assay. Maximum hemolysis was noted with Dx alone (15 μg/mL; 2.00 ± 0.11%) while the minimum was noted with α-TOS–CSH–MWCNTs/Dx (0.75 ± 0.11%). The rest of the formulations lie in between this range as can be seen in Fig. 8 (H). The findings suggested the safe and nonreactive charter of all the tested MWCNTs and unlikely to produce hemolysis (p > 0.05). These findings are in good correlation with our own
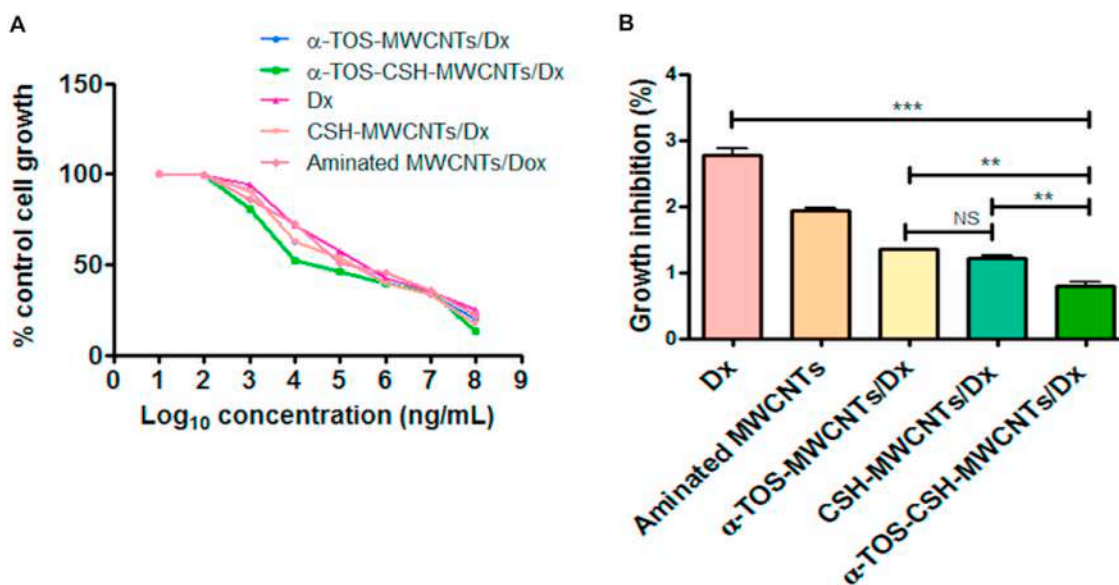

Fig. 6. (A) Kiton Red 620 assay of MDA-MB-231 cells treated with different MWCNTs formulations for 24 h. *Graph showing % cell growth vs. Log 10 concentration.* **(B) Growth inhibition GI$_{50}$ values for different treatment groups.** *Results are represented as Mean ± SD (n = 6).* (For interpretation of the references to color in this figure legend, the reader is referred to the Web version of this article.)
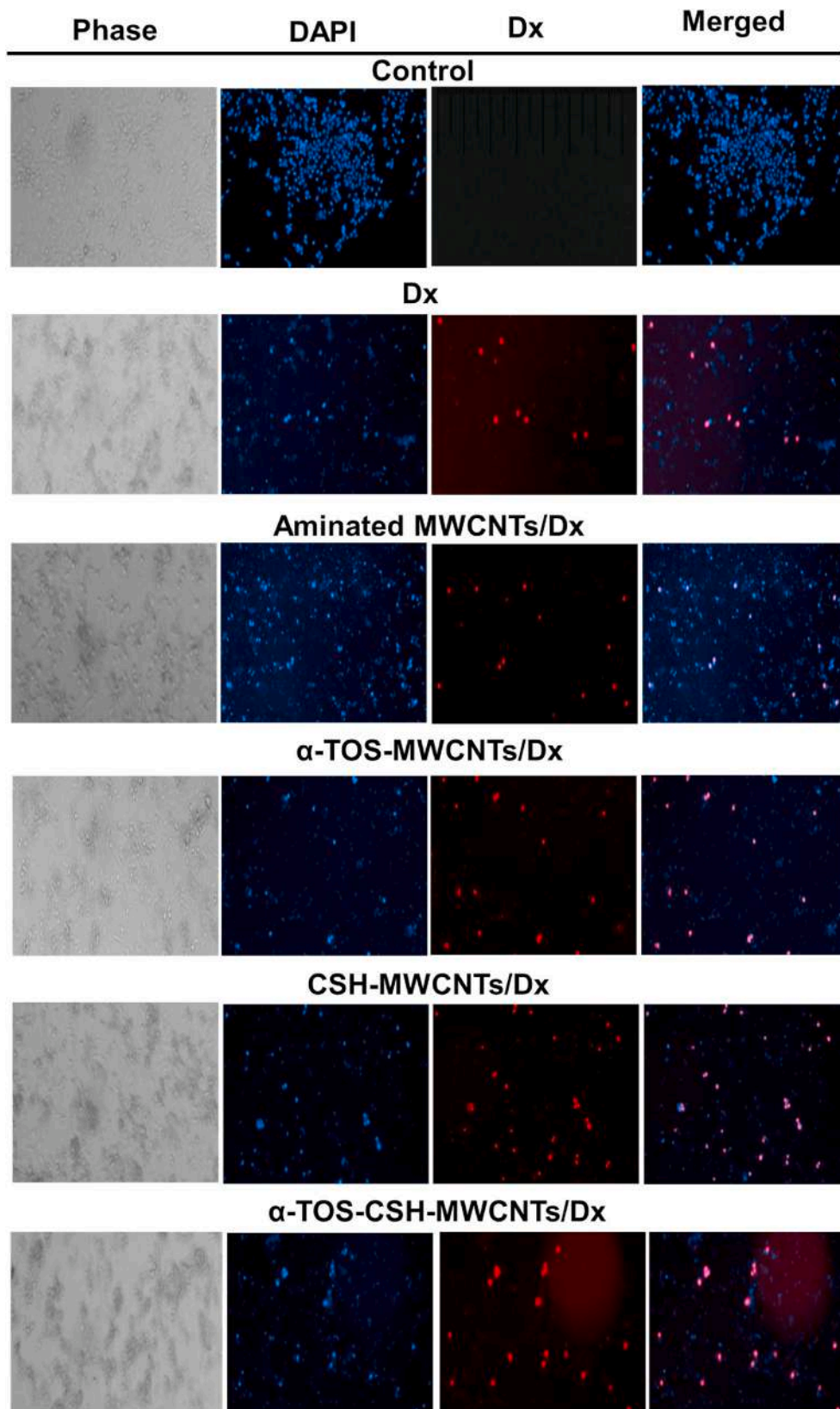
Fig. 7. Intracellular uptake of different treatment groups determined in MDA-MB-231 cells. CLSM was used to visualize the cellular uptake in MDA-MB-231 cells. *Scale bar:* 20 μm.
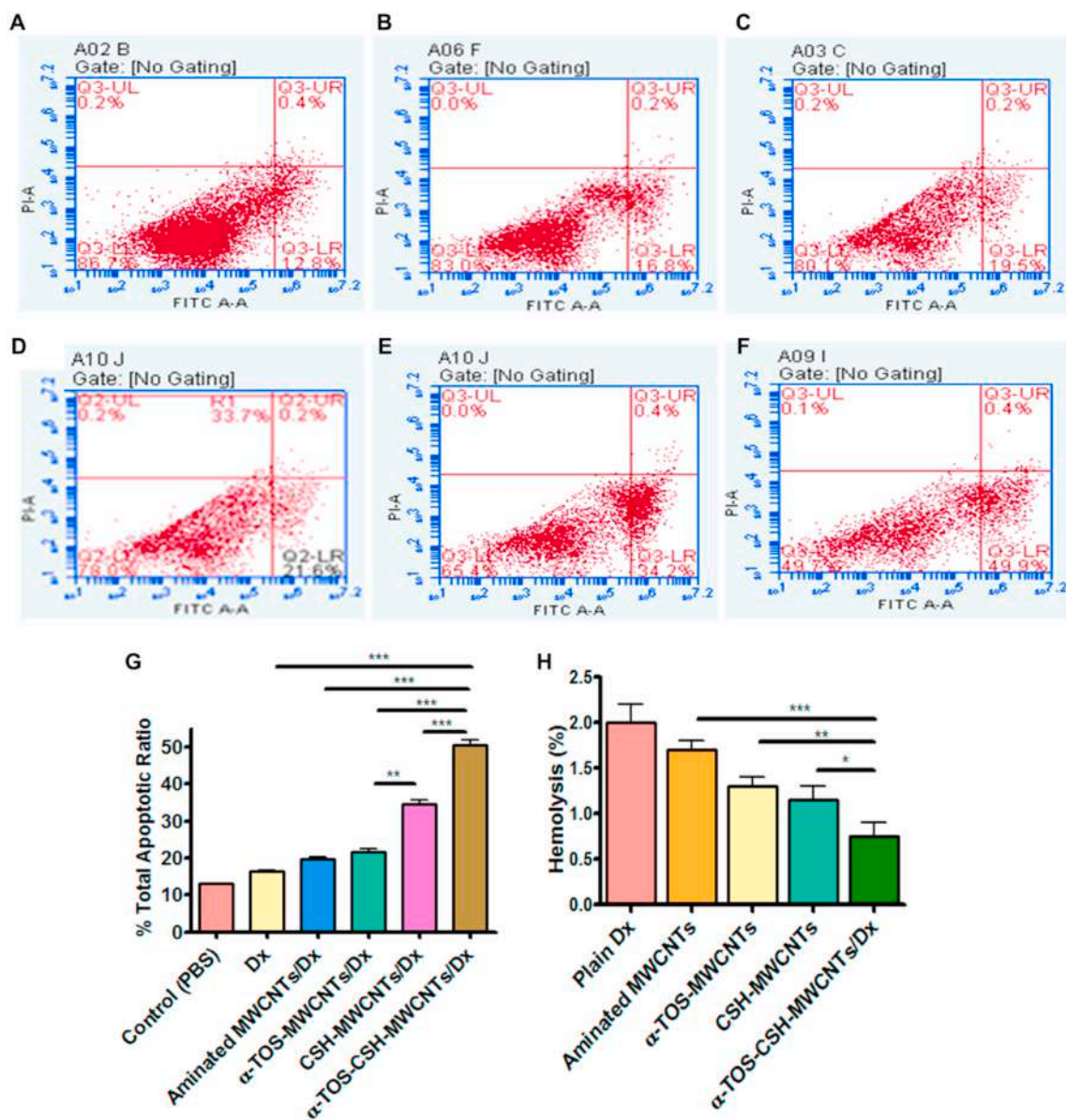
Fig. 8. A-F) % TCAR of MDA-MB-231 cells treated with different formulations was determined using the apoptotic assay. **(G)** Analysis of % TCAR using Image J software **(H)** Blood compatibility assay was carried out using Dx, NH₂-MWCNTs, α-TOS-MWCNTs, CSH-MWCNTs, and α-TOS–CSH–MWCNTs/Dx treated mouse blood. *Results are represented as Mean ± SD (n = 3).*

earlier reports [34].

3.12. Stability analysis of α-TOS–CSH–MWCNTs/Dx

Stability was accessed at $5 \pm 1\,°C$ and $30 \pm 2\,°C$ for 120 days and samples were collected on the day 1, 30, 60, 90 and 120 days and were

Table 1
Stability evaluation of NH₂-MWCNTs/Dx and α-TOS–CHS–MWCNTs/Dx dispersed in water at $5 \pm 1\,°C$ and $30 \pm 1\,°C$.

Formulation	Average size (nm)		PDI		Surface charge (mV)		% loading efficiency	
	Initial	After 120 days	Initial	After 120 days	Initial	After 120 days	Initial	After 120 days
$5 \pm 1\,°C$								
NH₂-MWCNTs/Dx	110.9 ± 2.96	176.5 ± 7.96	0.319 ± 0.067	0.587 ± 0.023	40.3 ± 3.2	32.5 ± 3.1	44.81 ± 2.1	26.34 ± 2.1
α-TOS-CSH-MWCNTs/Dx	132.1 ± 1.13	155.8 ± 3.49	0.229 ± 0.085	0.364 ± 0.054	31.5 ± 2.1	25.7 ± 3.1	75.90 ± 4.3	65.19 ± 3.0
$30 \pm 2\,°C$								
NH₂-MWCNTs/Dx	110.9 ± 2.96	218.3 ± 6.89	0.319 ± 0.067	0.673 ± 0.072	40.3 ± 3.2	30.1 ± 4.1	44.81 ± 2.1	20.11 ± 3.2
α-TOS-CHS-MWCNTs/Dx	132.1 ± 1.13	173.9 ± 4.98	0.229 ± 0.085	0.498 ± 0.067	31.5 ± 2.1	22.1 ± 3.7	75.90 ± 4.3	45.12 ± 5.1

Results are represented as Mean ± SD (n = 3).

evaluated for possible changes in size, PDI, surface potential and % drug leakage. As expected, significant ($P < 0.0001$) difference in size between day 1 to day 120 at 30 ± 1 °C was observed with all the formulations, whereas formulations were found quite stable at 5 ± 1 °C as comparatively very less difference (Table 1;*P > 0.005*) in size was observed. Particularly, NH$_2$-MWCNTs displayed a major change in size from 110.9 $\pm$ 2.96 to 218.3 $\pm$ 6.89 (almost twice the initial) in 120 days at 30 ± 1 °C. Alterations in PDI and surface charge were obtained in a similar line indicating the instability of NH$_2$-MWCNTs/Dx and α-TOS–CSH–MWCNTs/Dx at 30 ± 1 °C. The outcomes indicated that 30 ± 1 °C is not a suitable temperature condition for the storage of α-TOS–CSH–MWCNTs/Dx. Oppositely, findings at 5 ± 1 °C, displayed that NH$_2$-MWCNTs/Dx and α-TOS–CSH–MWCNTs/Dx were more stable in comparison to 30 ± 1 °C. Particularly, α-TOS–CSH–MWCNTs/Dx was found more stable than NH$_2$-MWCNTs/Dx in all respect (size, PDI, and Dx leakage). Our findings suggest that an enhancement in temperature from 5 ± 1 °C to 30 ± 1 °C leads to aggregation of MWCNTs, which subsequently resulted in enlargement in an average size and also disturb the homogeneity of the dispersion. Besides, findings also revealed that tailoring of the MWCNTs surface via α-TOS and CSH brings stability due to conjugate formation.

4. Conclusion

The developed CD44 receptor-targeted α-TOS–CSH–MWCNTs/Dx was successfully formulated and evaluated to treat TNBC. Dx was chosen to be the classical and proven anticancer drug. The idea was to effectively utilize the chemotherapeutic potential of Dx in combination with individual anticancer effect and targeting potential of α-TOS and CSH. Successive attachment of α-TOS and CSH and loading of Dx was confirmed via UV spectroscopy, FTIR spectroscopy, and NMR spectroscopic techniques. Dx loading and entrapment efficiency were notably improved upon conjugation with α-TOS and CSH. Higher cellular uptake of α-TOS–CSH–MWCNTs/Dx by MDA-MB-231 cells as determined using CLSM, indicative of effective CSH mediated CD-44 receptor targeting. In vitro anticancer efficacy as measured by Kiton Red 620 assay and apoptosis assay revealed the greater anticancer potential of Dx loaded MWCNTs decorated with α-TOS and CSH. Hemocompatibility evaluation ensures the safety of surface engineered MWCNTs as negligible interaction was observed with blood. Finally, the stability investigation suggests that refrigerator temperature (5 ± 1 °C) was better for the storage of α-TOS–CSH–MWCNTs/Dx as observed via measuring the changes in size, PDI, surface charge and % loading efficiency over 120 days.

This research work establishes the α-TOS and CSH mediated MWCNTs/Dx platforms as a synergistic therapy of TNBC. In the future, experimentation with additional cell lines, animal experiments, and toxicity profiling of developed formulation is required.

CRediT authorship contribution statement

Nidhi Jain Singhai: Conceptualization, Data curation, Investigation, Methodology, Writing - original draft, Funding acquisition. **Rahul Maheshwari:** Formal analysis, Writing - original draft, Writing - review & editing. **Narendra K. Jain:** Conceptualization, Formal analysis, Writing - review & editing. **Suman Ramteke:** Conceptualization, Project administration, Supervision, Formal analysis, Writing - review & editing.

Declaration of competing interest

The authors declare that they have no known competing financial interests or personal relationships that could have appeared to influence the work reported in this paper.

References

[1] G. Bianchini, J.M. Balko, I.A. Mayer, M.E. Sanders, L. Gianni, Triple-negative breast cancer: challenges and opportunities of a heterogeneous disease, Nat. Rev. Clin. Oncol. 13 (2016) 674.

[2] G. Prado-Vázquez, A. Gámez-Pozo, L. Trilla-Fuertes, J.M. Arevalillo, A. Zapater-Moros, M. Ferrer-Gómez, M. Díaz-Almirón, R. López-Vacas, H. Navarro, P. Maín, A novel approach to triple-negative breast cancer molecular classification reveals a luminal immune-positive subgroup with good prognoses, Sci. Rep. 9 (2019) 1538.

[3] H. Gonçalves Jr., M.R. Guerra, J.R. Duarte Cintra, V.A. Fayer, I.V. Brum, M. T. Bustamante Teixeira, Survival study of triple-negative and non–triple-negative breast cancer in a Brazilian cohort, Clin. Med. Insights Oncol. 12 (2018), 1179554918790563.

[4] Z. Sporikova, V. Koudelakova, R. Trojanec, M. Hajduch, Genetic markers in triple-negative breast cancer, Clin. Breast Canc. 18 (5) (2018) 841–850, https://doi.org/10.1016/j.clbc.2018.07.023.

[5] S. Al-Mahmood, J. Sapiezynski, O.B. Garbuzenko, T. Minko, Metastatic and triple-negative breast cancer: challenges and treatment options, Drug Deliv. Transl. Res. 8 (2018) 1483–1507.

[6] X. Dong, Z. Sun, X. Wang, X. Leng, An innovative MWCNTs/DOX/TC nanosystem for chemo-photothermal combination therapy of cancer, Nanomed. Nanotechnol. Biol. Med. 13 (2017) 2271–2280.

[7] M.A. Badea, M. Prodana, A. Dinischiotu, C. Crihana, D. Ionita, M. Balas, Cisplatin loaded multiwalled carbon nanotubes induce resistance in triple negative breast cancer cells, Pharmaceutics 10 (2018) 228.

[8] E.G. Graham, E.M. Wailes, N.H. Levi-Polyachenko, Multi-walled carbon nanotubes inhibit breast cancer cell migration, J. Biomed. Nanotechnol. 12 (2016) 308–319.

[9] S. Shilpi, S.U.R. Shivvedi, E. Gurnany, P. Chimaniya, A. Singh, M. Chouhan, S. Jain, S.K. Yagnik, K. Khatri, Chondroitin sulphate mediated targeted delivery of methotrexate and aceclofenac to the joints for effective management of rheumatoid arthritis, Asian J. Pharm. Pharmacol. 5 (2019) 495–502.

[10] S. Garg, A. Garg, S. Enaganti, A.K. Yadav, Chondroitin sulphate decorated polymeric nanoparticles: an effective carrier for enhancement of lung cancer targeting capabilities of anticancer drug, Curr. Nanomed. Recent Pat. Nanomed. 9 (2019) 243–261.

[11] D. Gurav, O.P. Varghese, O.A. Hamad, B. Nilsson, J. Hilborn, O.P. Oommen, Chondroitin sulfate coated gold nanoparticles: a new strategy to resolve multidrug resistance and thromboinflammation, Chem. Commun. 52 (2016) 966–969.

[12] N.J. Singhai, S. Ramteke, CNTs mediated CD44 targeting; a paradigm shift in drug delivery for breast cancer, Genes Dis. 7 (2020) 205–216.

[13] O.A. Ahmed, K.M. El-Say, B.M. Aljaeid, S.M. Badr-Eldin, T.A. Ahmed, Optimized vinpocetine-loaded vitamin e D-α-tocopherol polyethylene glycol 1000 succinate-alpha lipoic acid micelles as a potential transdermal drug delivery system: in vitro and ex vivo studies, Int. J. Nanomed. 14 (2019) 33.

[14] S. Tan, C. Zou, W. Zhang, M. Yin, X. Gao, Q. Tang, Recent developments in d-α-tocopheryl polyethylene glycol-succinate-based nanomedicine for cancer therapy, Drug Deliv. 24 (2017) 1831–1842.

[15] D. Matyszewska, E. Napora, K. Żelechowska, J.F. Biernat, R. Bilewicz, Synthesis, characterization, and interactions of single-walled carbon nanotubes modified with doxorubicin with Langmuir–Blodgett biomimetic membranes, J. Nanoparticle Res. 20 (2018) 143.

[16] H. Sadegh, G.A.M. Ali, S. Agarwal, V.K. Gupta, Surface modification of MWCNTs with carboxylic-to-amine and their superb adsorption performance, Int. J. Environ. Res. 13 (2019) 523–531.

[17] H.-j. Yao, Y.-g. Zhang, L. Sun, Y. Liu, The effect of hyaluronic acid functionalized carbon nanotubes loaded with salinomycin on gastric cancer stem cells, Biomaterials 35 (2014) 9208–9223.

[18] J. Zhu, L. Zheng, S. Wen, Y. Tang, M. Shen, G. Zhang, X. Shi, Targeted cancer theranostics using alpha-tocopheryl succinate-conjugated multifunctional dendrimer-entrapped gold nanoparticles, Biomaterials 35 (2014) 7635–7646.

[19] R.P. Singh, G. Sharma, S. Singh, M. Kumar, B.L. Pandey, B. Koch, M.S. Muthu, Vitamin E TPGS conjugated carbon nanotubes improved efficacy of docetaxel with safety for lung cancer treatment, Colloids Surf. B Biointerfaces 141 (2016) 429–442.

[20] N. SreeHarsha, R. Maheshwari, B.E. Al-Dhubiab, M. Tekade, M.C. Sharma, K. N. Venugopala, R.K. Tekade, A.M. Alzahrani, Graphene-based hybrid nanoparticle of doxorubicin for cancer chemotherapy, Int. J. Nanomed. 14 (2019) 7419.

[21] P.K. Pandey, R. Maheshwari, N. Raval, P. Gondaliya, K. Kalia, R.K. Tekade, Nanogold-core multifunctional dendrimer for pulsatile chemo-, photothermal-and photodynamic-therapy of rheumatoid arthritis, J. Colloid Interface Sci. 544 (2019) 61–77.

[22] F. Pareja, J.S. Reis-Filho, Triple-negative breast cancers–a panoply of cancer types, Nat. Rev. Clin. Oncol. 15 (2018) 347–349.

[23] N. D'Abreo, S. Adams, Immune-checkpoint inhibition for metastatic triple-negative breast cancer: safety first? Nat. Rev. Clin. Oncol. 16 (2019) 399–400.

[24] A. Gadeval, R. Maheshwari, N. Raval, D. Kalyane, K. Kalia, R.K. Tekade, Green graphene nanoplates for combined photo-chemo-thermal therapy of triple-negative breast cancer, Nanomedicine 15 (2020) 581–601.

[25] S. Mahajan, A. Patharkar, K. Kuche, R. Maheshwari, P.K. Deb, K. Kalia, R. K. Tekade, Functionalized carbon nanotubes as emerging delivery system for the treatment of cancer, Int. J. Pharm. 548 (2018) 540–558.

[26] K. Kuche, R. Maheshwari, V. Tambe, K.-K. Mak, H. Jogi, N. Raval, M.R. Pichika, R. K. Tekade, Carbon nanotubes (CNTs) based advanced dermal therapeutics: current trends and future potential, Nanoscale 10 (2018) 8911–8937.

[27] H. Jogi, R. Maheshwari, N. Raval, K. Kuche, V. Tambe, K.-K. Mak, M.R. Pichika, R. K. Tekade, Carbon nanotubes in the delivery of anticancer herbal drugs, Nanomedicine 13 (2018) 1187–1220.

[28] R.K. Tekade, R. Maheshwari, N. Soni, M. Tekade, Carbon Nanotubes in Targeting and Delivery of Drugs, Nanotechnology-Based Approaches for Targeting and Delivery of Drugs and Genes, 2017, pp. 389–426. Elsevier.

[29] L.-Y. Li, Y.-M. Zhou, R.-Y. Gao, X.-C. Liu, H.-H. Du, J.-L. Zhang, X.-C. Ai, J.-P. Zhang, L.-M. Fu, L.H. Skibsted, Naturally occurring nanotube with surface modification as biocompatible, target-specific nanocarrier for cancer phototherapy, Biomaterials 190 (2019) 86–96.

[30] X. Cao, L. Tao, S. Wen, W. Hou, X. Shi, Hyaluronic acid-modified multiwalled carbon nanotubes for targeted delivery of doxorubicin into cancer cells, Carbohydr. Res. 405 (2015) 70–77.

[31] Y. Yan, R. Wang, Y. Hu, R. Sun, T. Song, X. Shi, S. Yin, Stacking of doxorubicin on folic acid-targeted multiwalled carbon nanotubes for in vivo chemotherapy of tumors, Drug Deliv. 25 (2018) 1607–1616.

[32] O.P. Oommen, C. Duehrkop, B. Nilsson, J.n. Hilborn, O.P. Varghese, Multifunctional hyaluronic acid and chondroitin sulfate nanoparticles: impact of glycosaminoglycan presentation on receptor mediated cellular uptake and immune activation, ACS Appl. Mater. Interfaces 8 (2016) 20614–20624.

[33] P.S.O. Ozgen, S. Atasoy, B.Z. Kurt, Z. Durmus, G. Yigit, A. Dag, Glycopolymer decorated multiwalled carbon nanotubes for dual targeted breast cancer therapy, J. Mater. Chem. B 8 (15) (2020) 3123–3137, https://doi.org/10.1039/C9TB02711D.

[34] N.J. Singhai, R. Maheshwari, S. Ramteke, CD44 receptor targeted 'smart'multi-walled carbon nanotubes for synergistic therapy of triple-negative breast cancer, Colloid Interface Sci. Commun. 35 (2020) 100235.